6th International Conference on Advances in Experimental Structural Engineering
11th International Workshop on Advanced Smart Materials and Smart Structures Technology
August 1-2, 2015, University of Illinois, Urbana-Champaign, United States

Image Analysis for Crack Observation of a Cylinder RC Structure Cyclic Test

Y.S. Yang[1], H.C. Yang[2], Y.C. Chen[2] , H.J. Lu[2], C.C. Chang[2], C.L. Wu[3], T.T.C. Hsu[4]

1 *Associate Professor, Civil Engineering, National Taipei University of Technology, Taipei, Taiwan. E-mail: ysyang@ntut.edu.tw*
2 *Assistant Researcher, National Center for Research on Earthquake Engineering, Taipei, Taiwan.*
3 *Associate Researcher, National Center for Research on Earthquake Engineering, Taipei, Taiwan.*
4 *Moores Professor, Civil and Environmental Engineering, University of Houston, Houston, Texas, USA.*

ABSTRACT

The development of concrete surface cracks in an RC experiment is commonly observed and recorded by suspending a test at a few selected steps and sending inspectors to mark pen strokes on visible cracks. This work is labor intensive with a certain level of risk. An image analysis method was proposed to observe thin cracks of cylinder concrete surfaces, which has been implemented into a public software tool named ImPro Stereo. However, this method has never been verified by comparing image analysis results and labor pen marked cracks as it requires surface painting that may increase eye observation difficulty. This work compared the crack observation results observed by the image analysis method and labor pen marked cracks. The crack locations, widths, and lengths are compared. The limitations of both methods are discussed. A few strain concentration lines (probably cracks) that appeared in the very early stage of the test and observed by the image analysis method, before the labor pen marking was started, is presented and discussed in this paper.

KEYWORDS: *Tubular RC structure, cyclic test, crack observation, image analysis, ImPro Stereo*

1. INTRODUCTION

Crack observation is an important part of most of the reinforced concrete structural experiments. The crack patterns, angles, distribution density may reveal different failure modes, levels of damages, or stiffness degradation (Labib et al., 2013; Hsu & Mo, 2010). Cracks are typically observed by suspending a test, and sending inspectors to manually sketch lines on the surface of the cracks. However, this method can be time consuming, labor intensive, and risky at a certain level. In addition, a long experiment suspension could result in stress relaxation in the specimen, leading to inconsistent or inaccurate experimental results. Figure 1.1 shows the force relaxation observed in a pseudo-dynamic test of a double-skinned concrete-filled tubular (DSCFT) pier, which force dropped by 17% (from 198.6 kN to 165.5 kN) after a 1.5 hour suspension (Yang et al., 2007).

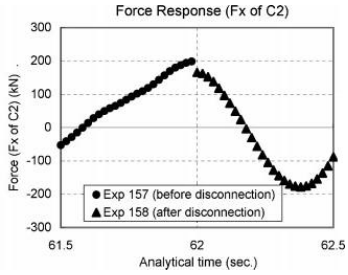

Figure 1.1 Force relaxation of a DSCFT pier after a 1.5-hour suspension (Yang et al., 2007)

As digital photography technology improves and hardware cost drops, image analysis offers a cost effective alternative way to observe concrete cracks. Not only the overall visual appearance of an experiment can be recorded, but also displacements, strain fields, cracks can be captured and analyzed. There have been many crack detection methods proposed (e.g., Adhikari et al., 2014). Most of them are based on edge detection methods that detect the dark shadow lines induced by cracks. These methods are valuable and practical for observing cracks which openings are wide enough to present dark lines in images. However, these methods are

limited if we are observing thin cracks that do not appear dark lines, or the cameras are located too far away from specimen to detect the dark lines. A preliminary image test (Figure 1.2) showed that a 0.15 mm crack (printed on a crack width ruler) or thinner is difficult to recognize by photos, even for photos taken by a high resolution digital camera (22 mega-pixel) at a close object distance (less than 2 meters).

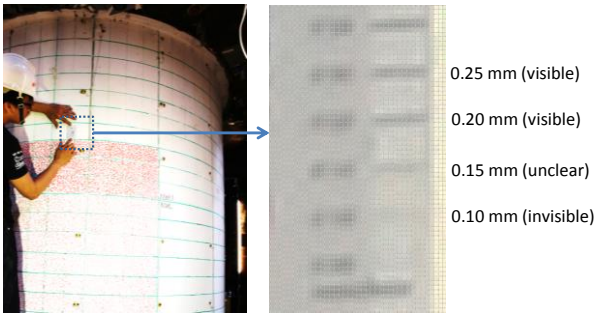

Figure 1.2 Minimal recognizable crack opening in photos taken in this test

This work estimated crack opening fields according to the image analyzed displacement fields. The crack opening can be seen as a related vertical displacement based on a rotated coordinate system. A displacement based image analysis is employed in this work to analyze the displacement field of the surface. This method has been developed by the authors of this paper and has been applied to many experiments (Yang et al. 2012; Yang et al. 2015). As the measured accuracy can achieve 0.04 pixels or even smaller (more accurate) if the lighting environment is good, the measured displacement field can be further derived to strain fields or crack distribution. This method has been applied to observe horizontal flexural cracks in an in-situ full-scale bridge pier test (Yang et al. 2015). This paper presents how the analysis formula is improved to observe 45-degree (and 135-degree) shear cracks. In addition, this paper also shows the crack opening comparison between manual estimation and image analysis.

2. ANALYSIS PROCEDURES AND FORMULAS

The image analysis method employed and modified in this work, which has been implemented in a MATLAB based and OpenCV (Bradski & Kaehler, 2008) powered program named ImPro Stereo (latest version updated in June 2015) (ImPro Stereo, 2015) generally consists of four major steps: stereo calibration of two cameras, 3D control point positioning, metric image rectification, and surface displacement analysis. Stereo calibration is to estimate the intrinsic and extrinsic parameters of cameras, including coordinate system transformation relationships between cameras, lens focus lens and distortion factors etc., providing sufficient parameters to carry out coordinate transformation between image coordinates and a 3D coordinate system. 3D control point positioning is to determine four control points of a part of a cylinder surface (named region of interests or ROI in this paper) by using sub-pixel template matching and stereo triangulation techniques (see Fig. 2.1).

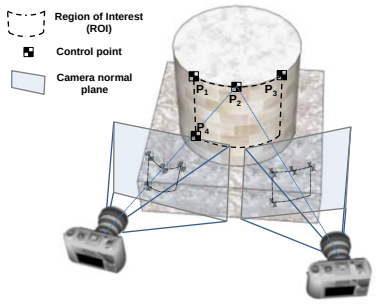

Figure 2.1 Control points positioning using stereo triangulation (Yang et al., 2015)

Metric rectification is then applied to convert the image of the ROI surface to a plane image through a series of resampling processes. Each resampling process generates a pixel, and the entire rectified image normally requires millions of resampling processes. Finally, the optical flow analysis is employed to analyze the displacement field. The details of the four steps can be found in literature (Yang et al. 2012; Yang et al. 2015) and is not repeated here.

The additional modification made in this work is to derive the crack opening field from the displacement field. As aforementioned, crack opening can be seen as the related vertical displacement in a rotated coordinate system. The analyzed displacement field is a discretized mesh, representing the displacement field of ROI. Each cell contains two numbers: Ux and Uy representing the horizontal and vertical displacement of a discrete cell. Figure 2.2 shows the crack opening model used in this work. A crack may induce a crack opening c_o and a crack sliding c_s. The crack separates a surface into two parts, say, part A and part B. By assuming the crack is ideally represented by two parallel lines in a small region (near around the cell marked **O** in Fig. 2.2), the crack opening is the smallest distance between the lines, while the crack sliding is the related movement parallel to the crack between two parts.

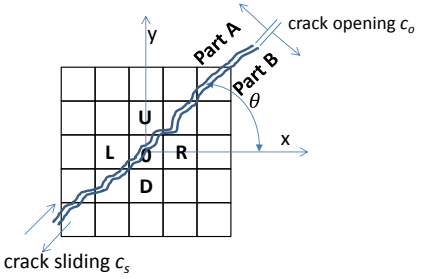

Figure 2.2 Crack opening model used in this work

Assuming the displacement fields around cell **O** is mainly induced by the crack, we ignore the deformation of parts A and B. The displacement of part A can be roughly estimated by a weighted average of cells U and L, while part B the cells R and D. The following equations are estimated while θ *is [0, 90^o)*:

$$U_A \cong \frac{U_U cos\theta + U_L sin\theta}{cos\theta + sin\theta} \tag{2.1}$$

$$U_B \cong \frac{U_D cos\theta + U_R sin\theta}{cos\theta + sin\theta} \tag{2.2}$$

While θ is *[90, 180^o)* the equations can be replaced with

$$U_A \cong \frac{-U_D cos\theta + U_L sin\theta}{cos\theta + sin\theta} \tag{2.3}$$

$$U_B \cong \frac{-U_U cos\theta + U_R sin\theta}{cos\theta + sin\theta} \tag{2.4}$$

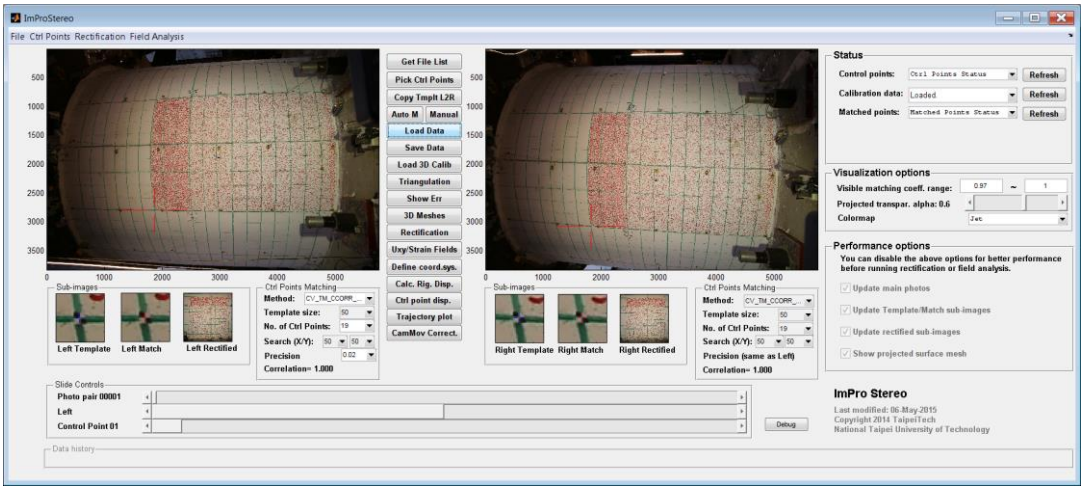

Figure 2.3 User interface of ImPro Stereo

The relationship between crack opening, sliding and displacements of parts A and B can be expressed by equation (2.5), where subscript *x* and *y* denote the *x* and *y* cmponenets, respectively.

$$\begin{bmatrix}\cos(\theta+\pi/2) & \cos\theta \\ \sin(\theta+\pi/2) & \sin\theta\end{bmatrix}\begin{bmatrix}c_o \\ c_s\end{bmatrix}=\begin{bmatrix}U_{Ax}-U_{Bx} \\ U_{Ay}-U_{By}\end{bmatrix} \tag{2.5}$$

The crack opening c_o of the cell O in Fig. 2.2 can be obtained by solving the 2-by-2 linear equations. The crack opening field can be estimated by calculating the crack opening cell by cell in the mesh.

The image analysis procedure has been implemented into software named ImPro Stereo (see Fig. 2.3). The latest version of the ImPro Stereo and instruction videos can be downloaded from https://sites.google.com/site/improstereoen/.

3. EXPERIMENTAL SETUP

The structural experiment in this work is a reinforced concrete cylinder tube subjected to a cyclic loading at its top. The height, outer diameter and thickness of the tube are 2.25 m, 2.5 m, and 0.15 m, respectively. The tube is fixed with rigid reinforced concrete blocks at its top and bottom. Figure 3.1 shows the dimensions and a photo of the specimen. The top reinforced concrete block is basically displacement controlled with a cyclic displacement history along a horizontal degree of freedom (say X) and controlled with zero rotations and torsion. A vertical load downward is applied by four vertical actuators to simulate the gravity load of the upper structure applied on the tube. The measurement includes 176 strain gauges attached on the reinforcing bars, 120 three-dimensional optical tracking points, and two sets of stereo imaging systems. This paper focuses on one of the stereo imaging systems, while other details of the experiment can be found in other literature and is not redundantly described in this paper.

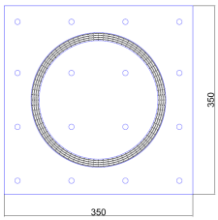

(a) Plan

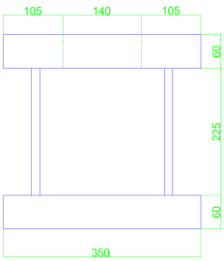

(b) Elevation

(c) Specimen and Setup

Figure 3.1 Specimen dimensions and photo

Two digital cameras were setup as a stereo imaging system at the north side of the specimen, aiming to measure the deformation and observe the crack distributions of the region of interests during the experiment. The region of interests occupies 1 eighth of the perimeter and half of the height, roughly was 0.98 m wide and 1.125 m high. The region of interests was painted with red random featured pattern for image analysis, as shown in Fig. 3.2 (a). The region was imaged by two cameras (Fig. 3.2 (b)) that were fixed on the strong floor and were remotely controlled by the controller, taking a pair of photos every five controlling steps of the experiment. However, there were other instrumentations and wires (mainly for optical tracking points) attached on the surface of the region of interests, which may result in image analysis noise. The noise induced by the wires can be seen later in the next section of this paper.

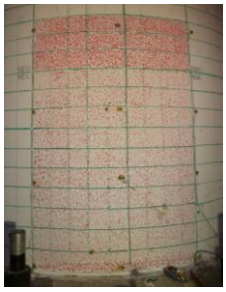

(a) Speckle marking for image measurement

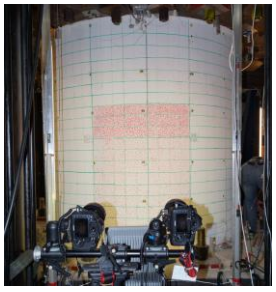

(b) Camera setup

(c) Other instrumentation contributing image noise

Figure 3.2 Imaging System Setup

4. ANALYSIS RESULT

The experiment applied a cyclic displacement history through 720 steps, as shown in Figure 4.1. The stereo imaging systems were triggered to take photos every five steps and at each peak of the displacement history (shown as green dots in Figure 4.1). There are totally 163 photo-taking steps. The experiment was suspended for crack marking for seven times, at drift ratio of 0.25%, -0.25%, 0.375%, -0.375%, 0.5%, -0.5%, and 0.75%. No further crack marking was done after that due to safety issue.

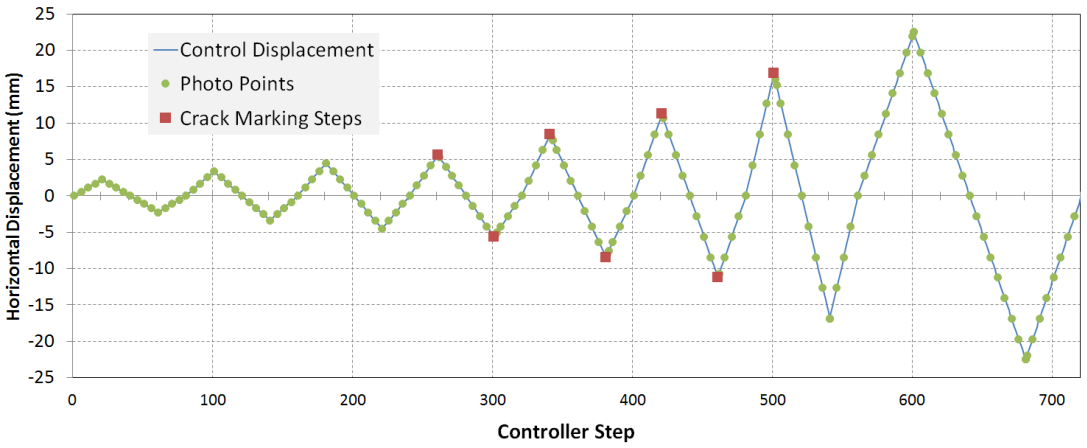

Figure 4.1 Cyclic history applied on the top of the specimen

Crack opening fields analyzed by ImPro Stereo based on the equations (2.1) to (2.5) aforementioned was carried out through the totally 163 photo-taking steps except the first step (as the first step is the initial condition). The theta is set to either 45 or 135 degrees according to the top displacement. What actually shown in crack opening fields are concentration lines of deformation. However, for brittle material like concrete, the authors believe the concentration lines of deformation are cracks. The crack opening fields provides a continuous crack development during the experiment. Due to the space limit, only a few crack opening fields are presented in this paper. Continuous crack development video generated in thi work can be examined at https://youtu.be/8ahXyU5DxOg

The image analysis of crack opening field (left plot of Fig. 4.2) presents that thin crack with only 0.03 mm opening width can be observed clearly by using the proposed method aforementioned in Section 3. Cracks with 0.02 mm opening can be observed as well. These cracks were observed when the drift ratio is 0.05%. The middle plot and right plots in Fig. 4.2 showed that it was just at the very beginning phase of the experiment, while the authors did not expect any cracks at this small drift ratio. However, these thin cracks are only invisible, and they actually exist. Neither naked eyes nor normal digital cameras can directly observe the dark lines of these thin cracks easily.

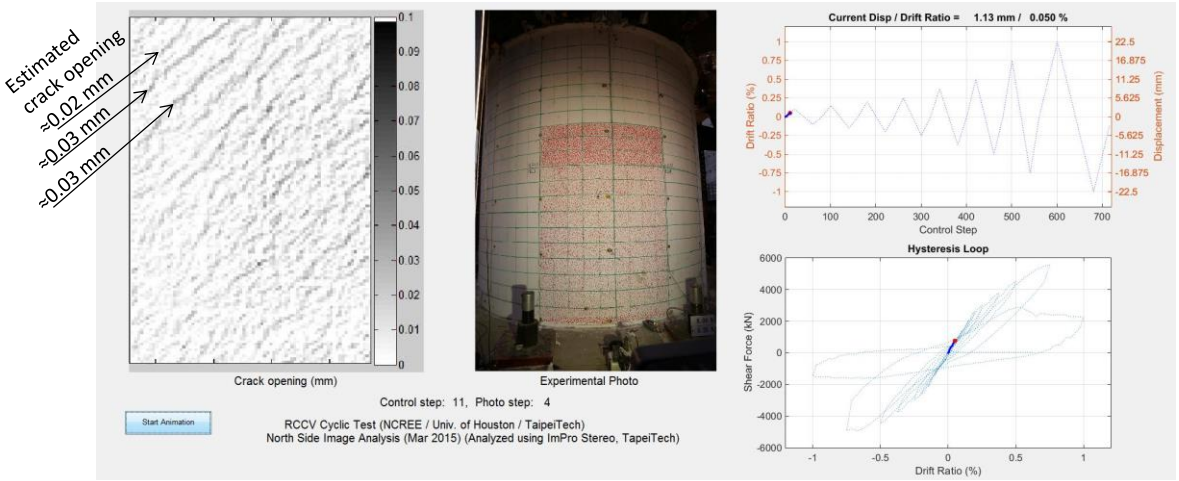

Figure 4.2 Thin cracks observed by image anlaysis (drift ratio: 0.05%)

Figure 4.3 shows the observed cracks while the drift ratio reached 0.1%. The thin cracks that were observed in Fig. 4.2 (while the drift ratio was 0.05%) became wider when the drift ratio reached 0.1%. More than ten cracks with openings from 0.02 to 0.05 mm were presented clearly. It should be mentioned that the authors did not expect any cracks while doing this experiment.

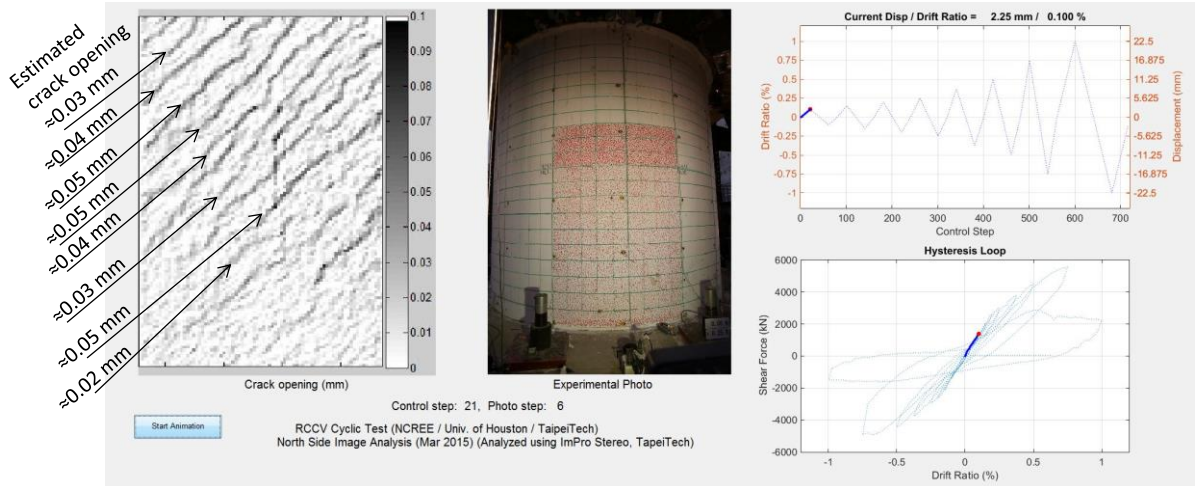

Figure 4.3 Thin cracks observed by image anlaysis (drift ratio: 0.1%)

The first crack marking suspension was while drift ratio reached 0.25%. Figure 4.4 (a) shows the crack marking pattern of the region of interests of the image analysis. To prevent interfering image analysis, the crack lines of the region of interests were marked on papers rather than directly on the concrete surface. All of the naked-eye visible cracks marked on the papers (totally 18 cracks) were clearly recognizable by using image analysis (Fig. 4.4 (b)). Most of the cracks were 0.1 mm or wider. Two additional cracks, tagged 19 and 20 in Fig. 4.4 (b), were analyzed by image but not recognized by naked eyes. Their widths were estimated 0.08 mm and 0.05 mm, respectively, which were thinner than most of the visible cracks. It could be the main reason that they were not invisible and were not marked on papers.

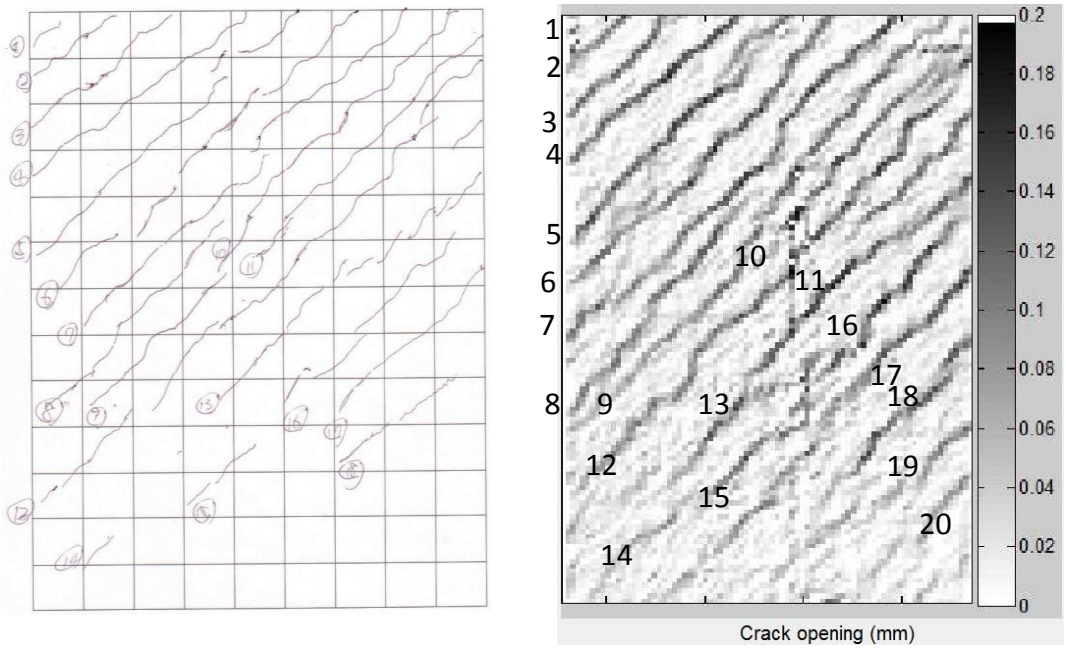

(a) Manual crack marking (b) Crack opening image analysis

Figure 4.4 Crack distribution: manual cracks marking vs. image analysis (drift ratio: 0.25%)

Crack opening widths can be estimated from both manual crack marking and image analysis. In manual marking, crack opening widths were estimated by using a crack width ruler. Table 4.1 lists the crack opening records that

were observed manually and by using image analysis. It should be mentioned that crack estimation by using a crack width ruler is not perfectly objective. Opening width of a long crack may vary at different parts of the crack. In addition, while crack width is as thin as 0.05 mm or 0.1 mm, it is not easy to tell the difference subjectively. Crack opening by image analysis is subjective as well. Analyzed crack opening is a field, like a mesh. It is subjective to determine which cells represent a crack. The crack openings by image analysis listed in Table 4.1 were the average of ten selected cells that have relatively larger opening values of a crack, while the cells were selected subjectively. Considering a certain level of subjective issues, the crack openings by manual estimation and image analysis roughly match with each other. The difference between manual estimation and image analysis is generally less than 0.03 mm and the maximal difference is 0.04 mm.

Table 4.1 Crack opening: manual cracks marking vs. image analysis (drift ratio: 0.25%)

Crack Tag	Crack opening (manual) (mm)	Crack opening (image) (mm)
1	0.1	0.07
2	0.1	0.09
3	0.1	0.10
4	0.15	0.14
5	0.1	0.14
6	0.1	0.13
7	0.1	0.14
8	0.1	0.11
9	0.1	0.09
10	0.15	0.12
11	0.15	0.13
12	0.05	0.08
13	0.1	0.12
14	0.05	0.08
15	0.1	0.12
16	0.15	0.13
17	0.15	0.13
18	0.1	0.10
19	(not recognized by naked eyes)	0.08
20	(not recognized by naked eyes)	0.05

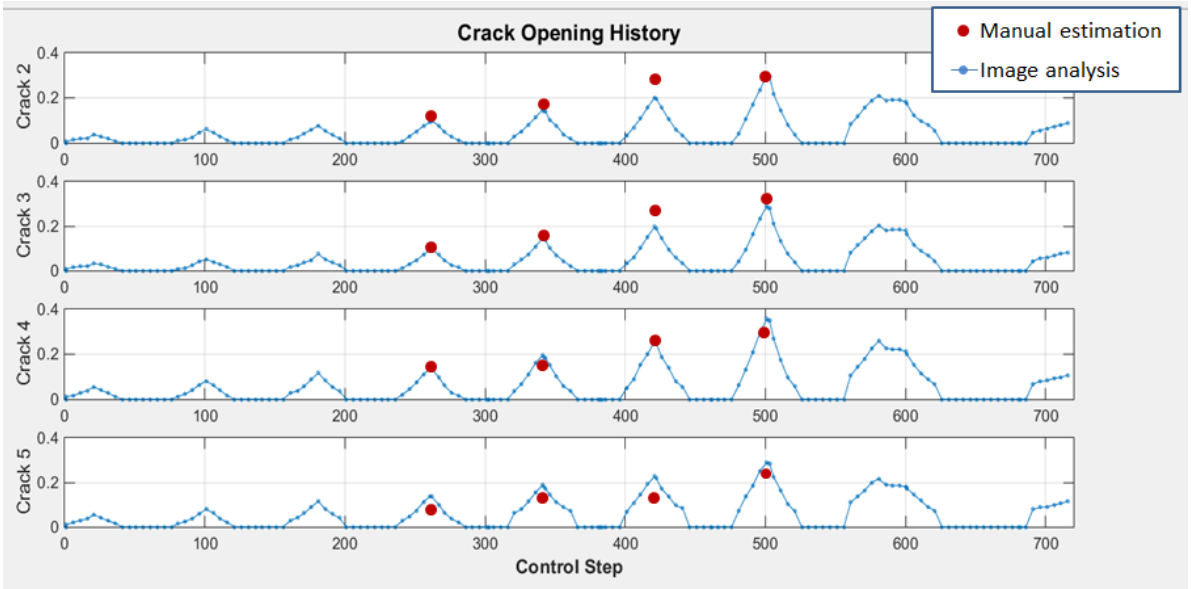

Figure 4.5 Estimated crack opening history of selected cracks

As there were 163 photographic steps in the experiment, the progress of crack development can be observed and visualized by generating a video. Unfortunately a video cannot be presented lively in this paper. Figure 4.5 presents variation of the crack opening widths of four selected cracks (i.e., tags 2, 3, 4, and 5 in Fig. 4.4) due to

limited space. By mapping with the controlling displacement in Fig. 4.1, it can be seen that the cracks opened when the actuator was pushing (i.e., while the displacement was positive) and closed when the actuator was pulling (i.e., while the displacement was negative). While these 45-degree cracks closed, other 135-degree cracks started to open (but are not shown in this paper due to limited space). The cracks were opening and closing in a surprisingly smooth way before about controller step 550. It became not so smooth after about step 550 mainly because a severe slipping failure started to occur. The slipping failure will be described in other papers and is not discussed here.

The image analysis was performed after the experiment off-line, not real-time analysis online. One of the reasons is the long computing it requires (which is about 3 hours in this case). Future efforts could address the employment of parallel computing such as GPU computing technique (e..g, Yang et al. 2015) to shorten the computing time of image analysis.

5. SUMMARY

This work performed image analysis to estimate the crack opening development of a reinforced concrete tubular structure subjected to a cyclic displacement at its top. Two sets of stereo imaging systems were setup in the experiment. The image analysis result of one of the systems (i.e., the north side one) was briefly presented in this paper. The crack opening fields were estimated by analyzing the displacement fields that were analyzed by image analysis implemented in ImPro Stereo.

Thin cracks that were as thin as 0.02 mm to 0.03 mm, which were still difficult to be seen by naked eyes, can be observed clearly by image analysis. Preliminary crack opening width comparison between manual estimation and image analysis showed that the differences were generally less than or equal to 0.03 mm. While manually marked cracks where available at only a few suspension steps (seven in this test), image analysis provides 162 steps of a continuous crack distribution and generated a video of crack changes. It also provides sufficient information to obtain crack opening width of any part of any selected crack at any selected experimental time point. The authors optimistically believe that image analysis offers an alternative, safe and efficient way to observe concrete cracks in cyclic tests.

AKCNOWLEDGEMENT

The authors acknowledge the research funding from National Center for Research on Earthquake Engineering (NCREE) and Ministry of Science and Technology, Taiwan. In addition, this experiment and the image analysis work cannot be successfully completed without great help from NCREE technicians and graduate students in National Taipei University of Technology, including C. C. Lin, S. Y. Wei, and S. J. Jheng.

REFERENCES

1. Labib, E., Mo, Y. L and Hsu, T.T.C. (2013). Shear Cracking of Prestressed Girders with High Strength Concrete, **Concrete Structures and Materials**, **7:1**, 71-78.
2. Hsu, T. T. C, and Mo, Y. L. (2010). Unified Theory of Concrete Structures. John Wiley & Sons.
3. Yang, Y. S., Hsieh, S. H., Tsai, K. C., Wang, S. J., Wang, K. J., Cheng, W. C., and Hsu, C. W. (2007). ISEE: Internet-based Simulation for Earthquake Engineering—Part I: Database approach, **Earthquake Engineering & Structural Dynamics**, **36:15**, 2291-2306.
4. Adhikari, R. S., Moselhi, O., and Bagchi, A. (2014). Image-based Retrieval of Concrete Crack Properties for Bridge Inspection, **Automation in Construction**, **39**, 180-194.
5. Yang, Y. S., Huang, C. W., & Wu, C. L. (2012), A Simple Image-based Strain Measurement Method for Measuring the Strain Fields in an RC-wall Experiment, **Earthquake Engineering & Structural Dynamics**, **41:1**, 1-17.
6. Yang, Y. S., Yang, C. M., and Huang, C. W. (2015), Thin Crack Observation in a Reinforced Concrete Bridge Pier Test using Image Processing and Analysis, **Advances in Engineering Software**, **83**, 99-108.
7. Bradski, G., and Kaehler, A. (2008). Learning OpenCV: Computer vision with the OpenCV library. O'Reilly Media, Inc.
8. ImPro Stereo Web site: https://sites.google.com/site/improstereoen/ (2015)
9. Yang, Y. S., Yang, C. M., and Hsieh, T. J. (2014), GPU Parallelization of an Object-Oriented Nonlinear Dynamic Structural Analysis Platform, **Simulation Modelling Practice and Theory**, **40**, 112-121.